forum acusticum 2026
8-12 September · Graz, Austria

INTERPRETABLE MACHINE LEARNING FOR ASSESSING ENVIRONMENTAL AND MOUNTING EFFECTS ON AERONAUTICAL GLASS WOOL ABSORPTION

Alfonso Caiazzo[1], Alessandro Casaburo[1], Giuseppe Petrone[1], Immacolata Climaco[2], Aurelio Bifulco[2]

[1] *PASTA LAB – Laboratory for Promoting Experiences in Aeronautical Structures and Acoustics, Department of Industrial Engineering, University of Naples Federico II, Naples, Italy*

[2] *Department of Chemical, Materials and Production Engineering (DICMaPI), University of Naples Federico II, Naples, Italy*

Abstract

Fibrous absorbers installed in aircraft fuselage linings are exposed to non-nominal mounting conditions and humidity variations that may alter their sound absorption performance. Although glass wool packages are commonly protected by surface layers, the combined influence of protective layers, installation-induced compression and moisture exposure remains only partially quantified under controlled impedance-tube conditions. This work investigates the acoustic variability of two aeronautical glass wool materials through sound absorption coefficient measurements performed over 250 Hz to 4250 Hz. Two experimental datasets are considered: the first examines material type, protective layer, mounting configuration and relative humidity, whereas the second addresses acoustic changes induced by repeated humidity cycles. Each factor is analyzed independently through a univariate neural-network classifier trained on pre-processed absorption curves. Classification accuracy is used as a qualitative indicator of feature detectability, while SHAP values identify the frequency regions responsible for the classification outcome. Results show that protective layers, material type, relative humidity and humidity cycles leave clear acoustic signatures, with univariate accuracies up to 99.5%, 96.0%, 69.6% and 82.5%, respectively. Installation effects are weaker but remain detectable above the random baseline. Humidity-cycle exposure produces progressive acoustic changes, supporting the relevance of moisture-driven degradation mechanisms in aircraft insulation systems.

Corresponding author: *alfonso.caiazzo@unina.it.*

Keywords: *Sound Absorption Coefficient, Aircraft Insulation, Environmental Effects, Installation Effects, Supervised Machine Learning*

1. Introduction

Fibrous porous absorbers are widely used in civil aircraft fuselage linings to improve cabin acoustic comfort while contributing to thermal insulation and fire-protection requirements [1]. In service, however, their acoustic response may deviate from nominal laboratory conditions because glass wool blankets are installed within complex insulation packages, often including protective layers and non-standard mounting constraints. Among the possible sources of variability, installation plays a critical role. Local compression, imperfect contact with the backing termination and operator-dependent handling can modify the effective thickness and porous microstructure of the material, thereby affecting the measured sound absorption coefficient. Previous studies showed that compression and mounting conditions may alter the acoustic response of fibrous absorbers [2]. Nevertheless, it remains unclear whether controlled mounting procedures with different contact-pressure distributions still produce distinguishable acoustic signatures. Environmental exposure represents an additional source of uncertainty. Protective layers can reduce direct exposure but do not necessarily prevent moisture uptake within the porous structure. Moreover, aircraft insulation packages undergo repeated humidity variations during successive flight phases, potentially inducing cyclic moisture absorption and desorption. Although humidity effects on porous materials have already been reported [3], the influence of relative humidity and repeated humidity cycling on aeronautical glass wool systems under

controlled mounting conditions and with protective layers remains insufficiently quantified.
This work experimentally investigates whether installation conditions, protective layers, relative humidity and humidity cycles produce distinguishable signatures in the sound absorption coefficient of aeronautical glass wool absorbers. Impedance-tube measurements are analyzed through a univariate supervised classification framework, in which each factor is considered independently. Classification accuracy is used as a qualitative indicator of factor detectability, while Shapley Additive Explanations (SHAP) identify the frequency regions that contribute most to the classification outcome. Further studies based on multivariate formulations are required to quantify possible interactions among the investigated factors.

2. Experimental methodology

2.1. Impedance tube measurements

The sound absorption coefficient, $\alpha(f)$, is measured using the two-microphone transfer-function method implemented in an impedance tube with 44 mm inner diameter, as shown in Fig. 1. The measurements are performed in accordance with ISO 10534-2 [4] and ASTM E1050-19 [5]. The investigated frequency range is 250 Hz to 4250 Hz.

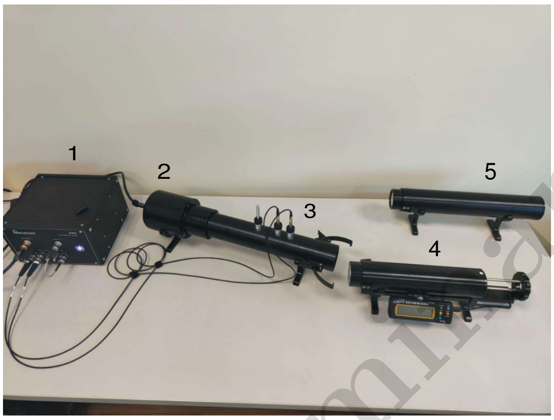

Figure 1: Impedance tube setup based on the two-microphone method: (1) data acquisition system, (2) loudspeaker, (3) microphones, (4) sample holder and (5) anechoic termination.

Two aeronautical glass wool absorbers are investigated: (i) green wool and (ii) grey wool. Both materials have a nominal thickness of 20 mm, while differing in fiber density, microstructural compaction and airflow resistivity. The materials are tested both with and without a protective layer in order to quantify the influence of the insulation package configuration.

2.2. Controlled mounting and humidification

A dedicated mounting fixture is used to impose repeatable contact conditions during specimen installation. The fixture consists of a plunger equipped with interchangeable terminations, as illustrated in Fig. 2. Three fixture-based configurations are considered: uniform pressure, localized pressure and finger pressure. The uniform configuration applies a spatially homogeneous load through a flat termination. The localized configuration applies discrete contact forces through four circumferentially distributed cylinders. The finger-pressure configuration reproduces a non-uniform contact pattern representative of manual handling, but in a geometrically controlled and repeatable form. The fingertip geometry has been reconstructed through a photogrammetry-based procedure and then converted into a solid model for manufacturing. A fourth condition, denoted as manual pressure, is obtained by direct operator installation without the mounting fixture.

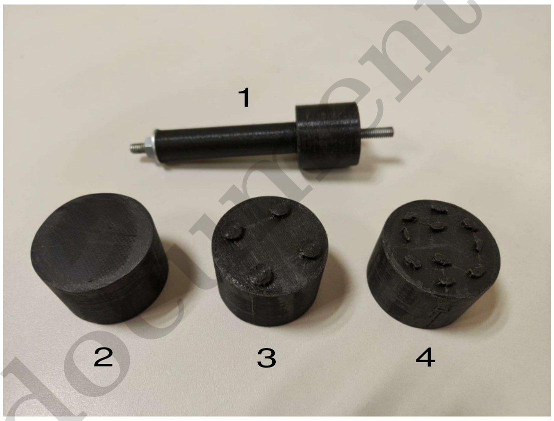

Figure 2: Mounting fixture used to impose controlled specimen installation conditions: (1) plunger, (2) uniform pressure termination, (3) localized pressure termination and (4) finger pressure termination.

The relative humidity of the specimens is controlled using a glove box (MBRAUN GB 2202-S). Dry nitrogen injection is used to regulate the internal atmosphere, while the temperature is maintained between 21 °C to 22 °C. Four relative humidity levels are considered: 10%, 40%, 70% and 100% RH. Each specimen is conditioned for 24 h before testing. For the 100% RH condition, the aim is to promote moisture uptake under saturated atmospheric conditions while avoiding direct contact with liquid water. After conditioning, the specimens are wrapped in aluminum foil and transferred to the impedance tube using moisture-buffering materials to limit unintended humidity variations.

2.3. Experimental datasets

Two datasets are considered in this work. The Installation and Environmental Variability Dataset, $\mathcal{D}_1$, is designed to investigate the effects of material type, protective layer, installation condition and relative humidity. The Humidity Cycling Degradation Dataset, $\mathcal{D}_2$, focuses on the acoustic evolution induced by repeated humidity cycles. The corresponding categorical factors are summarized in Table 1.
Dataset $\mathcal{D}_1$ includes measurements on three nominally identical specimens for each material–layer combination, resulting in twelve specimens. For each

Table 1: Categorical factors and classes considered in the two datasets.

Dataset	Factor	Classes
$\mathcal{D}_1$	Material	Green; Grey
	Layer	With; Without
	Installation	Uniform; localized; finger; manual
	RH level	10%; 40%; 70%; 100%
$\mathcal{D}_2$	Material	Green; Grey
	Humidity cycles	0; 1; 2; 3
	Specimen	1; 2; 3

investigated configuration, repeated impedance-tube measurements are performed and averaged to reduce random experimental variability. Dataset $\mathcal{D}_2$ is restricted to specimens equipped with the protective layer and installed using the uniform pressure configuration. Each humidity cycle consists of initial conditioning at 40% RH, exposure to 100% RH and final reconditioning at 40% RH before acoustic testing. Three consecutive cycles are applied after the reference state.

3. Univariate machine learning framework

3.1. Pre-processing and one-hot encoding

Before training, each absorption curve is pre-processed to reduce random fluctuations while preserving the dominant acoustic features. Following the procedure adopted in [6], a rolling-median smoothing with a 25-sample window is first applied. A rolling-maximum smoothing with a 50-sample window is then used to preserve the main absorption envelope. Finally, frequency-domain downsampling by a factor of 5 is applied to reduce the input dimensionality.

Each input sample corresponds to one pre-processed absorption curve,

$$\mathbf{x}_t = \left[\alpha_t(f_1), \alpha_t(f_2), \ldots, \alpha_t(f_{N_{\mathrm{freq}}})\right]^\top, \qquad (1)$$

where t identifies the measured curve and f_j is the j-th frequency bin. Therefore, each frequency point is treated as an input feature for the neural network. In the univariate formulation, each categorical factor is analyzed independently. For a selected factor, the corresponding class is represented using one-hot encoding. For example, if the relative humidity factor is considered with classes 10%, 40%, 70% and 100% RH, a specimen conditioned at 70% RH is encoded as

$$\mathbf{y}_{\mathrm{RH}} = [0, 0, 1, 0]^\top. \qquad (2)$$

Thus, a separate classifier is trained for each factor listed in Table 1.

3.2. Artificial neural network

The univariate method is based on a fully connected feed-forward artificial neural network. The architecture consists of an input layer, three hidden layers with 100, 50 and 25 neurons, respectively, and a softmax output layer. Rectified Linear Unit (ReLU) activation functions are used in the hidden layers. The output layer provides the class-membership probability associated with the selected factor.

For each univariate classification task, 75% of the observations are used for training and the remaining 25% for testing. Training is performed for 500 epochs using the ADAM optimizer [7]. Since the targets are one-hot encoded, the categorical cross-entropy loss is adopted:

$$\mathcal{L}(\hat{\mathbf{y}}, \mathbf{y}) = -\sum_{k=1}^{c} y_k \log(\hat{y}_k), \qquad (3)$$

where c is the number of classes of the considered factor, $\mathbf{y}$ is the ground-truth label and $\hat{\mathbf{y}}$ is the predicted probability vector. Classification accuracy is used to assess whether the selected factor leaves a detectable signature in the absorption curves. Accuracy values are interpreted with respect to the expected value.

3.3. SHAP-based interpretation

SHAP values are used to interpret the trained classifiers by quantifying the contribution of each input frequency to the model output [8], [9]. For a given curve t, class k and frequency bin f_j, the SHAP value $\phi_{t,k}(f_j)$ measures how the absorption value $\alpha_t(f_j)$ changes the predicted probability of class k with respect to its expected value. Positive SHAP values increase the probability assigned to the considered class, whereas negative values reduce it.

The class-specific SHAP values are used to identify the frequency regions that drive each univariate classification. Frequencies with large absolute SHAP values are interpreted as highly informative for discriminating the selected factor, whereas near-zero values indicate limited discriminative content. In this way, the ANN accuracy provides a qualitative measure of factor detectability, while SHAP analysis provides the corresponding frequency-dependent physical interpretation.

4. Results and discussion

4.1. Installation and relative humidity effects

The influence of mounting conditions is shown in Fig. 3. For specimens without the protective layer, both materials exhibit a monotonic increase of the sound absorption coefficient with frequency. The manual installation condition generally provides higher absorption values than the plunger-based configurations. Among the controlled plunger configurations, the uniform pressure termination produces the highest absorption coefficient, followed by localized and finger pressure. For Green Wool, the maximum variation between the uniform and finger pressure configurations reaches approximately 16% in the 1800 Hz to 4250 Hz range. For Grey Wool, a comparable variation is observed in the narrower 2000 Hz to 2800 Hz band.

When the protective layer is present, the installation-dependent trend is preserved but the spectral distribution changes. For Green Wool, the manual installation condition increases up to approximately 2200 Hz, followed by a plateau. The plunger-mounted configura-

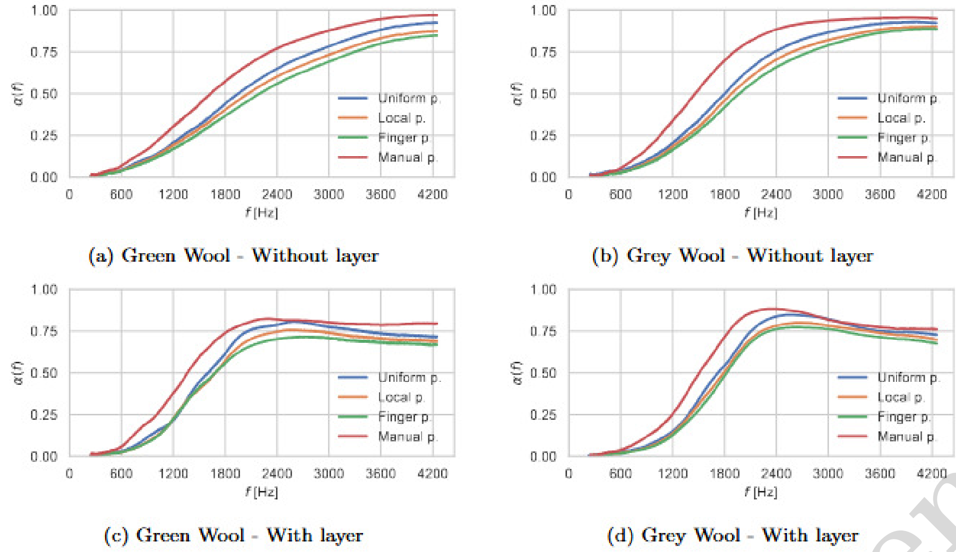

(a) Green Wool - Without layer

(b) Grey Wool - Without layer

(c) Green Wool - With layer

(d) Grey Wool - With layer

Figure 3: Effect of mounting conditions on the sound absorption coefficient for Green Wool and Grey Wool, with and without protective layer. Each curve represents the average of 27 measurements.

tions show lower peak absorption values, with maxima of approximately 0.78, 0.75 and 0.71 around 2600 Hz for uniform, localized and finger pressure, respectively. The largest variability among plunger configurations reaches approximately 22% in the 1800 Hz to 3000 Hz range. A similar but less pronounced behavior is observed for Grey Wool, with an average variation of about 16% in the 2000 Hz to 3000 Hz range.

These results suggest that the contact-pressure distribution imposed during installation affects the measured acoustic response. In particular, local compression may reduce the effective thickness of the specimen and promote partial pore closure, leading to changes in the absorption coefficient. Since no direct microstructural measurements are considered here, this interpretation should be regarded as physically plausible rather than directly demonstrated.

The effect of relative humidity is reported in Fig. 4. For specimens without protective layer, humidity-induced variations are mainly observed between 600 Hz to 3600 Hz. The maximum average differences between the most distant curves are approximately 22% for Green Wool and 26% for Grey Wool. In the presence of the protective layer, the spectral shape is modified and stationary points appear around 1720 Hz for Green Wool and 2020 Hz for Grey Wool. For Green Wool with layer, the average differences are approximately 17% before and 31% after the stationary point. For Grey Wool with layer, the corresponding values are about 8% and 26%, respectively.

The univariate classification results for dataset $\mathcal{D}_1$ are summarized in Table 2. Material type and protective layer are classified with accuracies of $96.0 \pm 2.05\%$ and $99.5 \pm 0.37\%$, respectively, largely exceeding the 50% random baseline. Relative humidity is also clearly detectable, with an accuracy of $69.6 \pm 3.83\%$ against a 25% baseline. Installation is less discriminative, but the obtained accuracy of $57.9 \pm 3.72\%$ remains above the 25% random level. This indicates that installation-dependent signatures are present, although weaker than those associated with material, protective layer and humidity. The reduced separability is consistent with the fact that part of the installation effect is concentrated in specific frequency regions and that the strongest contrast is likely associated with manual versus plunger-based configurations.

Table 2: Univariate classification accuracy for dataset $\mathcal{D}_1$.

Factor	Baseline	Accuracy
Material	50%	$96.0 \pm 2.05\%$
Protective layer	50%	$99.5 \pm 0.37\%$
Installation	25%	$57.9 \pm 3.72\%$
Relative humidity	25%	$69.6 \pm 3.83\%$

The SHAP analysis for installation and relative humidity is shown in Fig. 5. For the installation factor, non-negligible contributions are mainly concentrated below approximately 1500 Hz and in the 2000 Hz to 2400 Hz range. These regions correspond to portions of the spectrum where the absorption curves exhibit slope changes or localized deviations among mounting conditions. For relative humidity, the most informative bands are located below approximately 1300 Hz, between 2200 Hz to 3200 Hz and above 3600 Hz. This confirms that moisture-induced changes are frequency dependent and cannot be reduced to a uniform shift of the absorption curve.

4.2. Humidity-cycle-induced acoustic degradation

The effect of repeated humidity cycling is shown in Fig. 6. For both materials, differences among cycles are mainly observed in the 1800 Hz to 4250 Hz

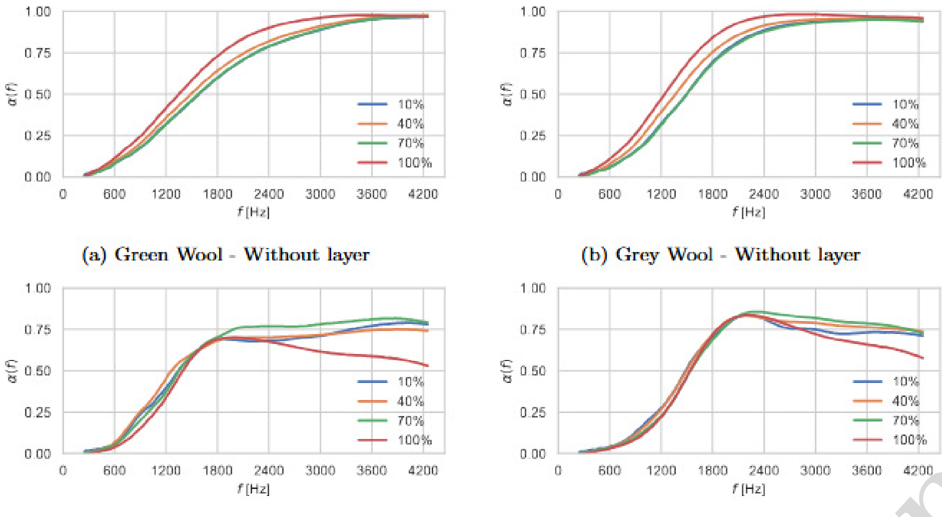

(a) Green Wool - Without layer (b) Grey Wool - Without layer

(c) Green Wool - With layer (d) Grey Wool - With layer

Figure 4: Effect of relative humidity on the sound absorption coefficient for Green Wool and Grey Wool, with and without protective layer. Each curve represents the average of 27 measurements.

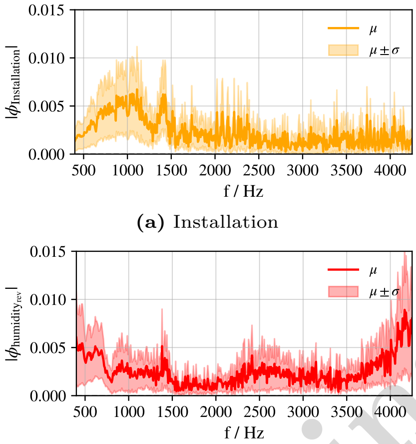

(a) Installation

(b) Relative humidity

Figure 5: SHAP values for dataset $\mathcal{D}_1$: (a) installation and (b) relative humidity.

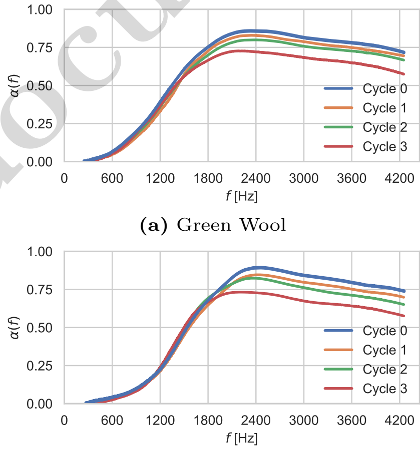

(a) Green Wool

(b) Grey Wool

Figure 6: Effect of humidity cycling on specimens with protective layer: (a) Green Wool and (b) Grey Wool.

frequency range. For Green Wool, the average differences between consecutive cycles are approximately 5% from cycle 0 to cycle 1, 3% from cycle 1 to cycle 2 and 13% from cycle 2 to cycle 3, with larger deviations in the high-frequency region. For Grey Wool, the corresponding values are approximately 4%, 3% and 15%, with larger deviations in the mid-frequency region. In both cases, the progressive change in the absorption curves indicates acoustic degradation associated with

Table 3: Univariate classification accuracy for dataset $\mathcal{D}_2$.

Factor	Baseline	Accuracy
Material	50%	$92.2 \pm 5.66\%$
Humidity cycles	25%	$82.5 \pm 6.33\%$
Specimen	33.3%	$42.2 \pm 7.1\%$

repeated humidity exposure.

The univariate classification results for dataset $\mathcal{D}_2$ are reported in Table 3. Material type is classified with an accuracy of $92.2 \pm 5.66\%$, confirming that the two glass wool materials remain distinguishable even when the protective layer and mounting configuration are fixed. Humidity cycles are classified with an accuracy of $82.5 \pm 6.33\%$, largely above the 25% random baseline. This result confirms that cyclic moisture exposure produces detectable acoustic signatures. The specimen classification accuracy is $42.2 \pm 7.1\%$, only moderately above the 33.3% random baseline, suggesting that specimen-to-specimen variability is not the dominant source of the observed acoustic changes.

The SHAP values associated with humidity-cycle classification are shown in Fig. 7. The most relevant contributions are concentrated below approximately 1300 Hz and above 3600 Hz. Compared with the relative humidity classification in dataset $\mathcal{D}_1$, the mid-frequency contribution is less pronounced. This suggests that instantaneous humidity level and repeated humidity cycling do not affect the absorption curves through identical spectral mechanisms. While relative humidity modifies several regions of the spectrum, cyclic exposure appears to generate stronger discriminative content at the lower and higher ends of the analyzed frequency range.

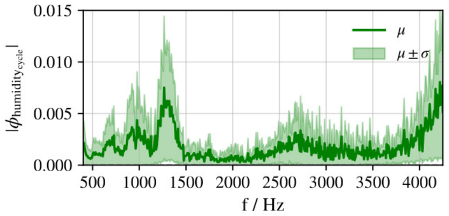

Figure 7: SHAP values obtained from the univariate classifier for the humidity-cycle factor in dataset $\mathcal{D}_2$.

5. Conclusions

This work investigated the acoustic variability of aeronautical glass wool absorbers subjected to different installation conditions, protective-layer configurations, relative humidity levels and repeated humidity cycles. Impedance-tube measurements were analyzed through a univariate neural-network classification framework, supported by SHAP-based interpretation to identify the frequency regions most affected by each factor.

The results show that material type, protective layer and relative humidity produce clearly distinguishable signatures in the sound absorption coefficient. Installation effects are weaker, but still detectable, indicating that the contact condition imposed during mounting can influence the measured acoustic response. These findings confirm that the acoustic behavior of glass wool absorbers cannot be fully described by nominal material properties alone, but depends on the actual mounting and environmental conditions.

A key outcome of the study is the evidence of progressive acoustic changes after repeated humidity cycling. Since the adopted cycles reproduce moisture variations that may occur during successive flight phases, this result suggests the presence of an acoustic fatigue phenomenon associated with humidity-induced material degradation. The effect is observed in both investigated glass wool materials and is sufficiently structured to be detected by the univariate classifier. Overall, the study highlights the need to account for humidity exposure and cyclic environmental loading when assessing the long-term acoustic performance of aircraft insulation systems. The proposed interpretable univariate framework provides a compact tool to detect degradation-related acoustic signatures and to support future investigations on the durability of porous absorbers under representative operating conditions.

6. Acknowledgments

The authors gratefully acknowledge Ida Giordano and Salvatore Ippolito for their contribution to the experimental measurement campaign carried out as part of their Bachelor's thesis work.

References

[1] Federal Aviation Administration, *Aircraft Materials Fire Test Handbook*. Washington, DC: U.S. Department of Transportation, FAA, 2000, DOT/FAA/AR-00/12.

[2] G. Petrone, A. Sorrentino, E. De Bono, T. Polito, F. Marulo, et al., "Installation effects on sound absorption and flow resistivity of glass wool fibres," in *Proceedings of ISMA 2018-International Conference on Noise and Vibration Engineering and USD 2018-International Conference on Uncertainty in Structural Dynamics*, KU Leuven-Departement Werktuigkunde, 2018, pp. 721–733.

[3] S. Yilmazer and M. B. Ozdeniz, "The effect of moisture content on sound absorption of expanded perlite plates," *Building and Environment*, vol. 40, no. 3, pp. 311–318, 2005. DOI: 10.1016/j.buildenv.2004.07.004.

[4] International Organization for Standardization, *ISO 10534-2:2023(E) Acoustics - Determination of sound absorption coefficient and impedance in impedance tubes - Part 2: Two-microphone technique for normal sound absorption coefficient and normal surface impedance*, Standard, Geneva, CH, 2023.

[5] E33 Committee, *ASTM E1050-19 Test Method for Impedance and Absorption of Acoustical Materials Using a Tube, Two Microphones and a Digital Frequency Analysis System*, 2019. DOI: 10.1520/E1050-19.

[6] M. Stender, C. Adams, M. Wedler, A. Grebel, and N. Hoffmann, "Explainable machine learning determines effects on the sound absorption coefficient measured in the impedance tube," *The journal of the Acoustical Society of America*, vol. 149, no. 3, pp. 1932–1945, 2021. DOI: 10.1121/10.0003755.

[7] E. Okewu, S. Misra, and F.-S. Lius, "Parameter tuning using adaptive moment estimation in deep learning neural networks," in *Computational Science and Its Applications–ICCSA 2020: 20th International Conference, Cagliari, Italy, July 1–4, 2020, Proceedings, Part VI 20*, Springer, 2020, pp. 261–272.

[8] S. Lundberg, "A unified approach to interpreting model predictions," *arXiv preprint arXiv:1705.07874*, 2017.

[9] M. Sundararajan and A. Najmi, "The many shapley values for model explanation," in *International conference on machine learning*, PMLR, 2020, pp. 9269–9278.